

Role of commensurate arrangements in the optical response of metallic gratings.

A. Barbara, J. Le Perchec, P. Quémerais, T. López-Ríos*
Institut Néel (CNRS/UJF), 25 avenue des Martyrs, BP 166, 38042 Grenoble Cedex 9, France

S. Collin, C. Sauvan, J-L. Pelouard
Laboratoire de Photonique et Nanostructures (LPN/CNRS), Route de Nozay, 91460 Marcoussis, France
 (Dated: November 26, 2021)

Light localization on commensurate arrangements of metallic sub-wavelength grooves is studied. We theoretically show that as the degree of commensuration tends to an irrational number new light localization states are produced. These have properties close to that reported for hot spots on disordered surfaces and are not permitted for simple period gratings. Some theoretical predictions are experimentally provided in the infra-red region by reflectivity measurements performed on two commensurate samples with respectively two and three slits per period.

PACS numbers: 71.36+c,73.20.Mf,78.66.Bz

Metallic systems such as random surfaces, thin films deposited on cold substrate or gratings, are known for their various and sometimes puzzling optical properties. In another context it is also known that quasi-crystals giving rise to a "forbidden" five-fold symmetry as well as one dimensional incommensurate structures may present electron localization effects[1, 2, 3, 4]. We thus expect new light localization effect by merging electromagnetic resonances of metallic surfaces and 1D incommensurate structures. The arrangements we study are sketched on fig.1. They are composed of several identical closed rectangular grooves per period separated by two possible sub-wavelength distances L (for long distance) and S (for short distance). The sequence of lengths, $LSSLS$ for instance, is chosen to be uniform and the arrangement is commensurate[4, 5, 6]. We can by this way study the optical properties of surfaces with complex topologies and interestingly we find that they present strong and sharp resonances associated to very local near-field intensity enhancements. Systems with N grooves per period, but separated by the same distance, have been theoretically studied[7, 8]. In the present context, they can be seen as particular cases of our commensurate structures given by the sequence of lengths $SSS..(\times N)L$. Up to three cavities per period, both approaches are equivalent. However, as grooves continue to be added our arrangements tend to a quasi-periodic (incommensurate) structure and both the near and far field properties become very different. Indeed, the commensurate arrangements present local, strong and wavelength dependency of the field localization inside the grooves. The near-field intensity distributions are associated to sharp cavity resonances which can be evidenced by dips in the reflectivity. An experimental prove of their existence is presented via reflectivity measurements performed in the infra-red region on gratings with respectively two and three slits per period. In that particular case, these measured modes also give the first experimental evidence of those predicted by Skigin et al.[9].

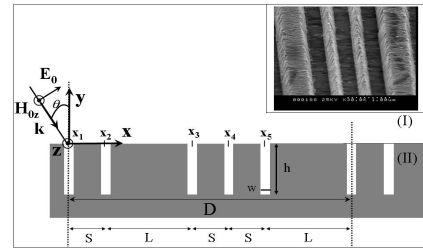


FIG. 1: Example of a uniformly ordered commensurate structure $\langle 3/5 \rangle$ of period $D = 3S + 2L$ where L and S respectively stand for the long and short distances separating two cavities. The grooves are identical with an aperture w and a height h . Inset represents a SEM image of the $\langle 2/3 \rangle$ sample.

The gratings of interest are characterized by a series $\{x_n\}_{1 \leq n \leq Q}$ of location of the center of the Q cavities contained in a period. The structures are generated fixing the origin at $x_1 = 0$ and using the equation[6]:

$$x_{p+1} = x_p + S \times \sigma_p + L \times (1 - \sigma_p)$$

$$\text{with } \sigma_p = [p \times R/Q] - [(p-1) \times R/Q]$$

where the function $[y]$ defines the integer part of y , R the number of grooves separated by the distance S and Q the number of grooves per period. These commensurate structures are called R/Q gratings, their period is $D = R \times S + (Q - R) \times L$ and the ratio R/Q indicates the order of commensurability. It is chosen to be an irreducible rational number. For example, the successive R/Q may be built by using the Fibonacci series $\{1, 2, 3, 5, 8, 13, \dots\}$ and take the values $\{1/2, 2/3, 3/5, 5/8, \dots\}$. For large R and Q the structure tends to a quasi-periodic (or incommensurate) one[6], $D \rightarrow \infty$, and $R/Q \rightarrow \xi = (\sqrt{5} - 1)/2$ the inverse of the mean gold number. We have calculated

the optical response of these structures illuminated by a p-polarized plane wave (magnetic field parallel to the groove) following the procedure detailed in ref[11]. The theoretical approach is an approximated modal method using the surface impedance boundary conditions[10], which has been several times successfully compared with experiments[12] when considering gold gratings with sub-micron geometrical parameters in the infra-red region. For commensurate gratings of period D the Rayleigh development of the field in the region (I) above the grating (fig.1) is:

$$H_z^{(I)}(x, y) = e^{ik(\gamma_0 x - \beta_0 y)} + \sum_{m=-\infty}^{m=+\infty} R_m e^{ik(\gamma_m x + \beta_m y)},$$

where $k = 2\pi/\lambda$ is the wave vector of the incident plane wave. The terms $\gamma_m = \sin\theta + m\lambda/D$, β_m defined as $\beta_m^2 = 1 - \gamma_m^2$, and R_m are respectively the normalized wave vectors and the amplitude of the m^{th} order of reflection. In region (II) the field is determined considering the vertical walls as perfectly conducting and applying the surface impedance approximation at the bottom of the cavity:

$$H_z^{(II)}(x, y) = \sum_{p=1}^Q \sum_{n=0}^{+\infty} A_p^n \cos \left[\frac{n\pi}{w} \left(x - x_p + \frac{w}{2} \right) \right] \times \left(e^{i\mu_n(y+2h)} + r_n e^{-i\mu_n y} \right) \Pi(x - x_p) \quad (1)$$

where $\Pi(x) = 1$ for $x \in [-w/2, w/2]$ and 0 elsewhere. A_p^n is the amplitude of the n^{th} mode in the p^{th} cavity with $\mu_n = k\sqrt{1 - (\frac{n\lambda}{2w})^2}$. The terms $r_n = (\mu_n/k + Z)/(\mu_n/k - Z)$, where $Z = 1/\sqrt{\varepsilon}$ and ε the dielectric constant of the metal, are the reflection coefficients of the n^{th} mode at the bottom of the cavity. Determining the coefficients A_p^n and R_n we find the electromagnetic field in the whole space. A_p^n is obtained by solving the matrix system:

$$\sum_{\ell=0}^{+\infty} \sum_{p'=1}^Q M_{n,\ell,p,p'} A_{p'}^\ell = V_p^n$$

$$\text{with } V_p^n = \left(\frac{2}{1 + \delta_{n,0}} \right) \frac{2\beta_0}{\beta_0 + Z} S_{0n}^+ e^{ik\gamma_0 x_p}$$

$$\text{and } M_{n,\ell,p,p'} = (e^{2i\mu_n h} + r_n) \delta_{n,\ell} \delta_{p,p'} - F_{n\ell} \sum_{m=-\infty}^{+\infty} \frac{S_{mn}^+ S_{m\ell}^-}{\beta_m + Z} e^{ik\gamma_m(x_p - x_{p'})}$$

where we have defined the terms S_{mn}^\pm and $F_{n\ell}$ as:

$$S_{mn}^\pm = \frac{1}{w} \int_{-w/2}^{+w/2} e^{\pm ik\gamma_n x} \cos \left[\frac{m\pi}{w} \left(x + \frac{w}{2} \right) \right] dx,$$

$$F_{n\ell} = \left(\frac{2}{1 + \delta_{n,0}} \right) \frac{w}{D} (e^{2i\mu_\ell h} - 1) \left(\frac{\mu_\ell}{k} + Z \right);$$

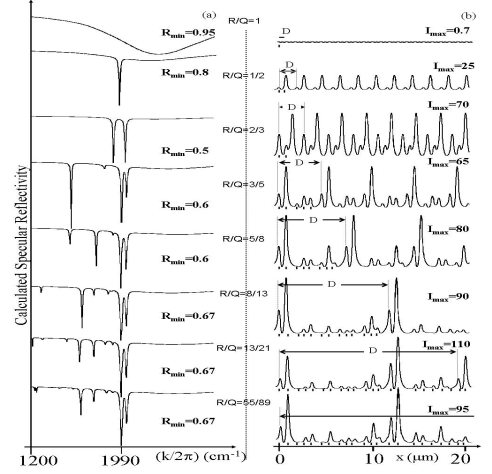


FIG. 2: (a) Specular reflectivity and (b) magnetic field intensity at the interface $y = 0$ at the frequency resonance located around 1990 cm^{-1} , calculated for several uniform structures as R/Q tends to the inverse of the mean golden number. Simulations were made with $h = 1\mu\text{m}$, $w = 0.3\mu\text{m}$, $S = 0.7\mu\text{m}$, $L = 1.2\mu\text{m}$ and an incidence angle $\theta = 15^\circ$. Vertical black lines in (b) indicate the position of the cavities within one period.

while R_n is given by:

$$R_m = \left(\frac{\beta_0 - Z}{\beta_0 + Z} \right) \delta_{m,0} + \frac{w}{D} \sum_{p=1}^Q \sum_{n=0}^{+\infty} A_p^n e^{-ik\gamma_n x_p} \times S_{mn}^- \left(\frac{\mu_n/k + Z}{\beta_m + Z} \right) (e^{2i\mu_n h} - 1).$$

Figure 2a displays the evolution of the specular reflectivity calculated at $\theta = 15^\circ$ as the order of commensurability tends to ξ . Simulations were made considering only the fundamental mode ($n=0$ in eq.1) and using the gold dielectric constant from ref[13]. For a simple-period grating, the spectrum presents the well-known broad dip due to the excitation of the Fabry-Perot like resonance inside the cavities[14]. As grooves are added, by considering the successive commensurate structures $1/2, 2/3, 3/5, 5/8$, supplementary and sharp resonances appear. For larger Q ($Q > 8$) only slight changes appear in the spectrum; the optical properties converge. In particular, one can see how the $< 8/13 >$ and the $< 55/89 >$ arrangements almost exhibit the same features. This is a direct indication of the self-similarity of the structures produced as $R/Q \rightarrow \xi$ [5]. The convergency of the optical properties lead to a situation where some strong and narrow resonances persist and are associated to strong local

fields. These properties are also direct consequences of the (in)commensurate character of the structure and do not exist for simple or compound gratings. Fig.2b shows the progressive establishment of hot spots, which are features experimentally observed on disordered metallic surfaces[16], as $R/Q \rightarrow \xi$. In the chosen configuration, the magnetic field intensity at the interface can locally be more than two orders of magnitude larger than the incident one (fig.2b) and this corresponds to enhancements of the electric field at the interface, larger than three orders of magnitude.

The occurrence of these new sharp cavity modes is due to the breaking of symmetry of the system. The pseudo-periodicity of symmetry of the fields remains valid for the global period D such that cavities within a period do not see the same exciting field and this opens up for different configurations. A physical image can be given by analogy to coupled dipoles. Indeed, in the case of a two-groove system a complete analytical study of the fields expression can be performed and allows to quantitatively characterize the nature of the resonances[15]: each resonating cavity acts as a damped oscillating dipole and their near-field coupling causes the splitting of each individual mode into a large one corresponding to the symmetric coupling of the cavities ($\rightarrow\rightarrow$) and a thin one, corresponding to the anti-symmetric coupling ($\rightarrow\leftarrow$). In the same manner, R/Q arrangements act as Q oscillating coupled dipoles, each mode corresponding to a specific configuration of the dipoles' orientation leading to more or less radiative modes and more or less intense near-field enhancements. Coupled modes of three slits with different individual frequency resonances were measured in the microwave regime[17]. Here, the Q cavities are identical but can still resonate at slightly different frequencies. A consequence is that the local intensity enhancements can be quite critically wavelength dependent. This property is also experimentally observed on disordered[16] or SERS (Surface Enhanced Raman Scattering) surface[18]. This point is illustrated in fig.3: maps of the electric field intensity along the x-axis and above a unit cell of a $\langle 8/13 \rangle$ grating are calculated for different incident wave-number scanned around the strong resonance located at 1990 cm^{-1} . Within a very narrow spectral range, here 1995 to 2038 cm^{-1} , the spatial localization of the electromagnetic field is strongly modified. For specific frequencies, one or few cavity(ies) act as active sites by almost individually concentrating very strong field intensity while the neighbouring ones are extinguished (fig3a and 3c).

To validate some of these theoretical results, we evidenced the existence of the sharp modes by measuring the specular reflectivity of gratings with one, two and three slits per period. The samples were prepared by electron-beam lithography and a double lift-off technique similar to ref.[19]: A Si substrate is first covered by a 200 nm-thick gold layer and secondly by a $1\text{ }\mu\text{m}$ -thick

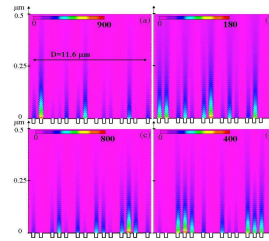


FIG. 3: Intensity maps of the electric field along the x-axis above one period of a $\langle 8/13 \rangle$ grating calculated at 1995 cm^{-1} (a) 2013 cm^{-1} (b) 2031 cm^{-1} (c) and 2038 cm^{-1} (d), with $\theta = 10^\circ$. $S = 0.7\text{ }\mu\text{m}$ and $L = 1.2\text{ }\mu\text{m}$ $h = 1\text{ }\mu\text{m}$ and $w = 0.3\text{ }\mu\text{m}$. The "jump" of photons localization is clearly seen, while the incident wave number varies of only a few percent.

Si_3N_4 layer deposited by plasma-enhanced chemical vapor deposition. Si_3N_4 walls of the width of the slits and separated either by the distance $L=1.2$ or $1.5\text{ }\mu\text{m}$ or $S=0.7\text{ }\mu\text{m}$, are performed by electron-beam lithography and reactive ionic etching. A 650 nm-thick gold layer is then deposited, and the Si_3N_4 walls are lifted-off by means of a HF solution. The obtained grooves have a trapezoidal shape ($w_{\text{down}} = 0.36\text{ }\mu\text{m}$ and $w_{\text{top}} = 0.62\text{ }\mu\text{m}$) while rectangular grooves are considered in the model. Small discrepancies between some nominal values and those used in the calculations are attributed to this shape difference. Grating area are $2 \times 2\text{ mm}^2$. Reflectivity measurements of p-polarized impinging light were performed at room temperature, in dry air, in the 1.67 to $6\text{ }\mu\text{m}$ spectral range, with a BioRad FTS60A DigiLab Fourier Transform photospectrometer. Spectra were normalized to the reflectivity of a flat gold surface. Figure 4 displays reflectivity measurements and calculated spectra realized at $\theta = 10^\circ$. Parameters used in the calculation are: $h_{\langle 1/1 \rangle} = 0.64\text{ }\mu\text{m}$, $D = 2.2\text{ }\mu\text{m}$, $h_{\langle 1/2 \rangle} = 0.69\text{ }\mu\text{m}$, $S = 0.7\text{ }\mu\text{m}$, $L = 1.5\text{ }\mu\text{m}$, $h_{\langle 2/3 \rangle} = 0.6\text{ }\mu\text{m}$, $S = 0.65\text{ }\mu\text{m}$, $L = 1.3\text{ }\mu\text{m}$ and $w = 0.55\text{ }\mu\text{m}$ for all samples. Figure 4a shows the previously measured large cavity mode noted CM as well as the $n = \pm 1$ branches of the surface plasmons noted SP[11]. These SP occurs around the same wave number for the two other gratings since the period of the three samples have close values. More interestingly, the splitting of the large CM into the two predicted resonances for the $\langle 1/2 \rangle$ grating and into three predicted resonances for the $\langle 2/3 \rangle$ grating is measured. The three resonances of $\langle 2/3 \rangle$ correspond to the symmetric coupling of the three cavities ($\rightarrow\rightarrow\rightarrow$), the symmetric coupling of the two external cavities, anti-symmetric to the central one whose dipole momentum is twice

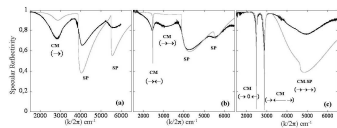


FIG. 4: Measured (black line) and calculated (light gray line) specular reflectivity at $\theta = 10^\circ$ of the gratings $\langle 1/1 \rangle$ (a), $\langle 1/2 \rangle$ (b) and $\langle 2/3 \rangle$ (c). Cavity resonances are noted CM and surface plasmon SP. The arrows indicate the direction of the equivalent dipole momentum at the mouth of each cavity.

larger ($\rightarrow \leftarrow \rightarrow$) and the anti-symmetric coupling of the external cavities leading to the extinction of the field in the central one ($\rightarrow 0 \leftarrow$).

To highlight the symmetric or anti-symmetric nature of the two sharp resonances of the $\langle 2/3 \rangle$ grating, we have performed reflectivity measurements at various angles. Increasing θ breaks the symmetry of the system and favors the excitation of the anti-symmetric mode which vanishes at normal incidence (the symmetric incident field cannot couple to it). Figure 5 evidences the turnaround of the strength of two resonances as a function of the incidence angle and demonstrates that peak at smaller wave number is the anti-symmetric mode ($\rightarrow 0 \leftarrow$): it is weakly excited at small incidence angles and grows to become predominant around $\theta = 33^\circ$. Opposite behaviour is observed for the symmetric dip. Modifying the incident angle may thus be an easy way to control the near-field distribution.

In conclusion, theoretical study of commensurate gratings tending to incommensurate structures was used to model and understand the optical properties of metallic surfaces with complex topologies. Thanks to these structures we can generate, in a controlled manner, weakly radiative modes which localize local, strong and wavelength dependant electromagnetic fields. These features are of great interest since they are commonly admitted to occur on disordered and/or SERS surfaces. Finally, experimental evidence of these modes was given in the infra-red region for simple commensurate structures.

The authors would like to thank Nathalie Bardou for assistance in the fabrication process.

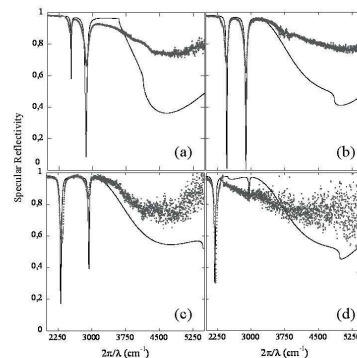


FIG. 5: Experimental (black line) and calculated (gray line) specular reflectivity of the $\langle 2/3 \rangle$ grating performed at $\theta = 4^\circ$ (a), $\theta = 12^\circ$ (b), $\theta = 24^\circ$ (c) and $\theta = 33^\circ$ (d). Calculations are made considering four modes in the cavities.

* aude.barbara@grenoble.cnrs.fr;

- [1] C. Berger, E. Belin, D. Mayou, *Ann. Chim. Mater. (Paris)* **18**, 485 (1993).
- [2] E. Belin, D. Mayou, *Phys. Scr.* **T49**, 356 (1993).
- [3] G. de Laissardiere, D. Nguyen-Manh, D. Mayou, *Prog. Mater. Sci.* **50**, 679 (2005).
- [4] S. Aubry and P. Quémerais in *Low-dimensional electronic properties of Molybdenum bronzes and oxides*, p.293 (Ed. C. Schlenker, Kluwer Academic publishers 1989).
- [5] F. Ducastelle, *Order and phase stability in alloys*, Cohesion and Structure vol. 3, (Ed. F.R. De Boer, D. G. Pettifor, North-Holland 1991).
- [6] F. Ducastelle, P. Quémerais, *Phys. Rev. Lett.* **78**, 102 (1997).
- [7] D. C. Skigin and R. A. Depine, *Phys. Rev. Lett.* **95**, 217402 (2005) and references therein.
- [8] D. C. Skigin and R. A. Depine, *Phys. Rev. E* **74**, 046606 (2006).
- [9] D. C. Skigin, A. N. Fantino and S. I. Grosz, *J. Opt. A: Pure Appl. Opt.* **5**, 129 (2003).
- [10] A. Wirgin, A.A. Maradudin, *Prog. Surf. Sc.*, **22**, 1 (1986).

- [11] A. Barbara, P. Quémerais, E. Bustarret, T. López-Ríos, T. Fournier, *Eur. Phys. Jour.* **D**, 23, 143 (2003).
- [12] A. Barbara, P. Quémerais, J. Le Perchec and T. López-Ríos, *J. Appl. Phys.* **98**, 033705 (2005).
- [13] E. D. Palik, *Handbook of Optical Constants of Solids*, Academic Press.
- [14] T. López-Ríos, D. Mendoza, F. J. García-Vidal, J. Sánchez-dehesa and B. Pannetier, *Phys. Rev. Lett.* **81**, 665 (1998).
- [15] J. Le Perchec, P. Quémerais, A. Barbara and T. López-Ríos, *Phys. Rev. Lett.* **97**, 036405 (2006).
- [16] S. Ducourtieux et al., *Phys. Rev. B* **64**, 165403 (2001).
- [17] A. P. Hibbins, I. R. Hooper, M. J. Lockyear, J. R. Sambles, *Phys. Rev. Lett.* **96**, 257402 (2006).
- [18] M. Moskovits, *Rev. Mod. Phys.* **57**, 783 (1985).
- [19] S. Collin, F. Pardo, R. Teissier and J-L. Pelouard *Appl. Phys. Lett* **85**,194 (2004).